KeAi
CHINESE ROOTS
GLOBAL IMPACT

Contents lists available at ScienceDirect

Petroleum Science

journal homepage: www.keaipublishing.com/en/journals/petroleum-science



Original Paper

The investigation of multiple factors on elastic anisotropy of artificial shale based on the orthogonal experiment



Fei Gong ^a, Liang-Liang Gao ^b, Guan-Gui Zou ^{a, *}, Su-Ping Peng ^a, Yi-Chen Song ^b

- ^a College of Geoscience and Surveying Engineering, China University of Mining and Technology (Beijing), Beijing, 100083, China
- ^b State Key Laboratory of Petroleum Resources and Prospecting, China University of Petroleum (Beijing), Beijing, 102249, China

ARTICLE INFO

Article history: Received 3 August 2022 Received in revised form 15 January 2023 Accepted 13 April 2023 Available online 1 May 2023

Edited by Jie Hao

Keywords: Shale Elastic anisotropy Multiple factors Orthogonal design

ABSTRACT

Elastic anisotropy of shales is critical to accurate constraints for rock physical models, quantitative interpretation and hydraulic fracturing. However, the causes of elastic anisotropy of shales are very complicated, and the understanding of how multiple influence factors affect the elastic anisotropy of shales is still not clear. Hence, the orthogonal experiment, as an effective multiple factors experimental method, is adopted in this study to analyze the effect of multiple factors for shale elastic anisotropy. Three factors, clay content, organic matter (OM) content and compaction stress are selected as independent variables, the orthogonal test table $L_{16}(4^3)$ with four levels for each factor is adopted. According to the designed orthogonal table, sixteen artificial shales are constructed based on the cold-pressing method, and all the dry artificial shales are measured by the ultrasonic measurements. The influence of each factor on the elastic anisotropy and the sensitivity orders of three factors are obtained using the range analysis. The orders of sensitivity for selected factors follow the sequence clay content > compaction stress > OM content for velocity anisotropy parameters. The compaction mechanism of artificial shales is also discussed by the compaction factor, which are positively correlated with the velocity anisotropy parameters. The clay platelets orientation distribution function (ODF) of samples is evaluated by a theoretical model, the ODF coefficients are significantly affected by the clay content and compaction stress, and W_{200} are much more sensitive to these factors than W_{400} . The results can provide a critical rock physics basis for quantitative interpretation and reservoir prediction of the low-maturity or maturity shale reservoir.

© 2023 The Authors. Publishing services by Elsevier B.V. on behalf of KeAi Communications Co. Ltd. This is an open access article under the CC BY-NC-ND license (http://creativecommons.org/licenses/by-nc-nd/4.0/).

1. Introduction

Elastic anisotropy of shales is critical to accurate constraints for rock-physical models, quantitative interpretation and hydraulic fracturing (Allan et al., 2015). The presence of the clay mineral and kerogen can significantly affect the intrinsic elastic anisotropy of shales (Vernik and Nur, 1992; Sayers, 2013; Sondergeld and Rai, 2011; Vasin et al., 2013; Pan et al., 2018). Clay mineral, as the main component of shales, can affect the intrinsic elastic properties via the clay type, volume content, and the orientation distribution (Mondol et al., 2007, 2008; Voltolini et al., 2009; Sayers et al., 2015; Gong et al., 2020; Ding et al., 2021). Clay platelets in shales tend to display obvious alignment during the diagenetic process due to

their layered structure (Moyano et al., 2012), causing complex variations for elastic anisotropy of shales (Kawamura and Ogawa, 2004; Sayers and den Boer, 2019). Although several theoretical and experimental studies have been investigated the influence of clay on the shale elastic properties and provided qualitatively convincing results (Vernik and Liu, 1997; Hornby, 1998; Wenk et al., 2007; Sarout and Guéguen, 2008; Sayers, 2013; Gong et al., 2020), the effect of clay mineral is still not well explained due to its complexity.

Organic matter (OM) is a crucial variable that affecting the intrinsic anisotropy of shales, which can affect the elastic properties via the type of OM, volume content and thermal evolution degree (Bandyopadhyay, 2009; Prasad et al., 2011; Sayers, 2013; Zargari et al., 2013; Yenugu, 2014; Li et al., 2015; Zhao et al., 2016; Xie et al., 2019). Clarifying the correlation between the OM and elastic properties of shales is pivotal to understand the induced mechanisms of anisotropy and can provide potential relationship

E-mail address: cumtzgg@foxmail.com (G.-G. Zou).

^{*} Corresponding author.

F. Gong, L.-L. Gao, G.-G. Zou et al.

Petroleum Science 20 (2023) 2773–2783

for indication of "sweet spot" from seismic data. However, quantitatively characterizing the shale elastic anisotropy is still challenging because the properties of OM vary significantly according to their origin such as thermal evolution degree and distribution.

Due to multiple influence factors caused by the complex multicomponent in natural shales, it is impossible to separate and individually investigate the effect of these parameters such as clav and OM content on the intrinsic elastic anisotropy of shales. Therefore, most of experimental studies on elastic anisotropy of shales are conducted on artificial shales to separate and investigate effects of these parameters individually (Luan et al., 2016; Altowairqi et al., 2015; Beloborodov et al., 2016, 2018; Xie et al., 2019; Gong et al., 2020). The artificial shales can overcome substantial limits on measurements due to the limited available quantity, strong heterogeneity, chemically and mechanically unstability of natural shale samples. However, previous artificial shales mainly focused on the effects of single variable such as the OM content, clay type and content, which are inconsistent with the multiple influence factors for the elastic anisotropy of shales. Note that the influence factors of shales anisotropy can be affected by each other. For example, compaction and diagenesis can reduce the porosity, and alter the alignment of clay minerals and OM (Wang, 2002; Yang and Guo, 2020). The understanding of how multiple influence factors affect the elastic anisotropy of shales is still not clear.

As an effective multiple factor experimental method, the orthogonal design test is adopted in this study to analyze the effects of multiple influence factors for intrinsic elastic anisotropy of artificial shales. Three factors, clay content, OM content, and compaction stress are selected as independent variables, and sixteen artificial shales are constructed based on the orthogonal experimental. The impact of the selected influence factors on the elastic anisotropy of artificial shales are analyzed, and the influence factors are ranked by the range analysis. The ODF of clay platelets is also derived to quantitatively characterize the impact of the alignment of clay platelets on the elastic anisotropy for the artificial shales. The results can help to understand how multiple influence factors affect the elastic anisotropy of shales and may be used to estimate how the elastic anisotropy evolve due to burial of the low-maturity or maturity shale reservoir.

2. Sample preparation and measurements

For Yanchang shales in the Ordos Basin, OM is in a stage of low-maturity and illite is the dominant clay mineral, which is a major shale oil reservoirs in China (Kun et al., 2020; Ding et al., 2021). Natural shales are mainly composed of clay minerals, quartz, carbonate minerals and organic matter, which constitute more than 95% of shale, and these components are responsible for its major properties (Wang, 2002; Sone and Zoback, 2013; Luan et al., 2016; Gong et al., 2020). However, it is extremely difficult to separate and investigate the effect of these multiple influence factors individually for natural shales due to their complex multi-component. Therefore, the artificial shales are constructed in this study to simulate natural shales, which allow parameters such as the component and compaction to be controlled.

To simulate the Yanchang shales, the quartz, illite, calcite and OM are chosen to construct the artificial shales. The OM are extracted from natural rocks to ensure the properties of artificial shales agree with the natural shales. Type II kerogen with relatively low vitrinite reflectance ($R_0 = 1.2$) are extracted from natural rocks to ensure the properties of artificial shales agree with the natural

shales. The purity of illite meets the requirements of the experiment from the X-ray diffraction analysis (Gong et al., 2020). However, the accurate elastic properties of clay minerals and OM is still a long-standing problem although several studies published some data. Quartz and calcite are the common brittle minerals in shales, the bulk and shear moduli of quartz is K=37 GPa, $\mu=44$ GPa, K=76.8 GPa, $\mu=32$ GPa, while K=37 GPa, $\mu=44$ GPa, K=76.8 GPa, $\mu=32$ GPa with calcite, respectively (Mavko et al., 2020).

As an effective multiple factor experimental method, the number of experiments can be reduced by utilizing an orthogonal array (Xi et al., 2019; Yao et al., 2021). Taking a 3-factors 3-levels design as an example, the number of tests can be effectively reduced from 27 to 9 as shown in Fig. 1. Therefore, the orthogonal design is adopted to investigate the influence of multiple factors on the elastic anisotropy of artificial shales. As mentioned above, the main influence factors are clay mineral, OM and the platelet-shaped pores which can be affected by the compaction and diagenesis. Therefore, three factors, the clay content (factor A), OM content (factor B), and the compaction stress (factor C) are selected as independent variables, each factor has four levels (Table 1). The detail orthogonal experiment table is L_{16} (4^3), which adopts constant calcite content and the interchange between increasing OM content and decreasing quartz content for each case (Table 2). Based on the orthogonal experiment table, sixteen artificial shales each with different compaction stress, clay and OM content are constructed.

The artificial shale samples are constructed by cold-pressing method (Gong et al., 2020). Firstly, the powder mixture is mixed in a ball mill to ensure a homogeneous composition, and then homogeneous powder is mixed with liquid adhesives to simulate the cementation of natural shales. Secondly, the powder-adhesive mixture is stuffed into a specially designed mold and is undergoing a certain uniaxial effective stress for more than 100 h, then could be removed from the mold (Fig. 2a). The more details procedure can be found in Gong et al. (2020). To further reduce the influence of epoxy resin on physical and elastic of artificial rocks, 3% epoxy resin are used, which is less than the weight content used in Gong et al. (2020).

The porosity and bulk density of dry artificial shales are obtained by He pycnometry and envelope-volume determination, respectively. The velocities of dry artificial shales are measured by the ultrasonic transmission test at the room condition using 0.5 MHz Pand S-wave transducers. The homogeneity and transverse isotropy of the artificial shales constructed by our method have been validated in previous studies, and the details can be found in Luan et al. (2016) and Gong et al. (2018). Since full stiffness constants of artificial shales should be measured in three directions: normal and parallel to bedding, and at an angle 45° to bedding. Therefore, sixteen artificial shales are cut at 45° with respect to the bedding as shown in Fig. 2b. Then the velocities in three directions can be obtained based on the ultrasonic measurements, and the measurements error is be less than 1%. Note that the artificial shales are firstly heated to 70 °C for more than 48 h to get the "relatively" dry samples, and then are placed in the room condition for 24 h to contain about 2-3% water to compensate the influence of water loss from clay dehydration on the damage to the rock framework.

The scanning electron microscopy (SEM) observations of sample A13 are obtained using an FEG Quanta 200F and reveal considerable texture with layering of clay mineral, the laminated structures of artificial shales can be found visually from fresh surfaces (Fig. 3). Due to the uniaxial effective stress are applied during the construction process, the structure of the artificial shale reveals that

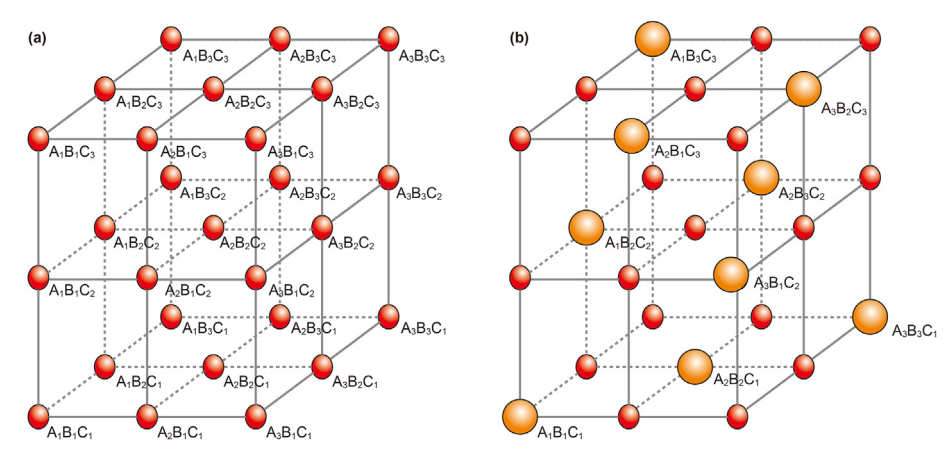


Fig. 1. The sketches for (a) uniform and (b) orthogonal experimental designs. The red spheres represent the tests for uniform experimental design and the orange spheres represent the tests for orthogonal experimental design in 3-factors 3-level design.

Table 1The selected influence factors with four levels. As independent variables, factor A and factor B is the clay and OM content, respectively, factor C is the compaction stress.

Level	Factor A, %	Factor B, %	Factor C, MPa
1	20	4	75
2	30	6	100
3	40	8	125
4	50	10	150

Table 2 Orthogonal experiment table $L_{16}\ (4^3)$ with three factors and four levels. As independent variables, factor A and factor B is the clay and OM content, respectively, factor C is the compaction stress. A1—A16 represent the sample (test) number.

Sample	Factor A, %	Factor B, %	Factor C, MPa	Quartz, %	Calcite, %
A1	20	4	75	60	16
A2	20	6	100	58	16
A3	20	8	125	56	16
A4	20	10	150	54	16
A5	30	4	100	50	16
A6	30	6	75	48	16
A7	30	8	150	46	16
A8	30	10	125	44	16
A9	40	4	125	40	16
A10	40	6	150	38	16
A11	40	8	75	36	16
A12	40	10	100	34	16
A13	50	4	150	30	16
A14	50	6	125	28	16
A15	50	8	100	26	16
A16	50	10	75	24	16

the clay platelets are almost aligned the bedding plane on the micro-scale, which can cause a strong elastic anisotropy to artificial shales. Unlike the complex discontinuity of shale laminae, most cracks also aligned along the bedding plane.

3. Theoretical background

The elasticity and anisotropy have been discussed in several studies, hence only a brief introduction is necessary in this study. With reference to a vertical transverse isotropy (VTI) media, since $C_{12} = C_{11} - 2C_{66}$, the elastic properties can be determined by only five independent stiffness constants:

$$C_{ij} = \begin{bmatrix} C_{11} & C_{12} & C_{13} & & & \\ C_{12} & C_{11} & C_{13} & & & \\ C_{13} & C_{13} & C_{33} & & & \\ & & & & C_{44} & & \\ & & & & & C_{66} \end{bmatrix}$$
(1)

Oľ

$$S_{ij} = \begin{bmatrix} S_{11} & S_{11} - S_{66}/2 & S_{13} \\ S_{11} - S_{66}/2 & S_{11} & S_{13} \\ S_{13} & S_{13} & S_{33} \\ & & & S_{44} \\ & & & & S_{66} \end{bmatrix}$$
(2)

with

$$S = C^{-1} \tag{3}$$

One purpose of this paper is to study the elastic anisotropy from five independent stiffness, which can be calculated from the Christoffel equation as follows (Dewhurst and Siggins, 2006):

$$C_{11} = \rho V_{P(90^{\circ})}^2,$$
 (4)

$$C_{33} = \rho V_{P(0^{\circ})}^{2}, \tag{5}$$

$$C_{44} = \rho V_{\text{SV}(0^{\circ})}^{2},\tag{6}$$

$$C_{66} = \rho V_{SH(90^{\circ})}^{2}, \tag{7}$$

and

$$\begin{split} C_{13} &= -C_{44} \\ &+ \sqrt{\left(C_{11} + C_{44} - 2\rho V_{P(45^{\circ})}^{2}\right) \left(C_{33} + C_{44} - 2\rho V_{P(45^{\circ})}^{2}\right)}, \end{split} \tag{8}$$

where ρ represents the bulk density of rocks; the direction of wave propagation in Eqs. (4)–(8) correspond to the angle with the symmetry axis of VTI media.

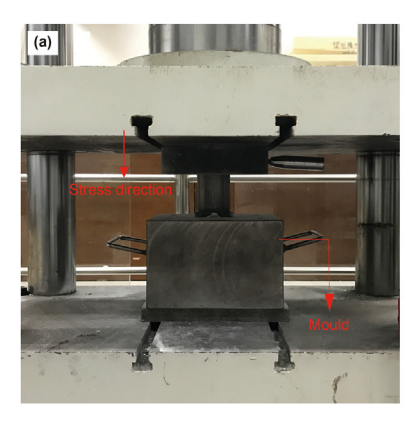
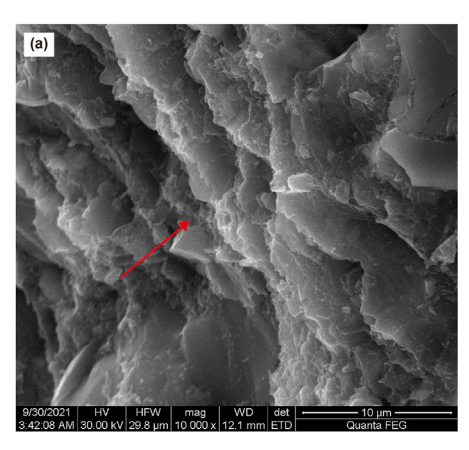




Fig. 2. (a) Stress consolidation process of artificial shales and (b) the artificial shales after cutting.



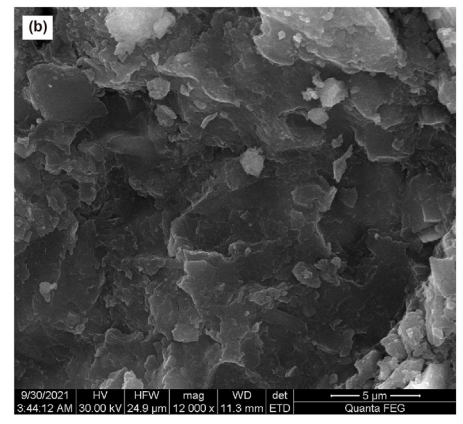


Fig. 3. SEM pictures of artificial shale A13 (a) parallel to the bedding plane (b) perpendicular to the bedding plane. The arrows indicate the bedding plane or lamination.

According to Thomsen (1986), the anisotropy parameters can be obtained from the five dynamic elastic constants as following:

$$\varepsilon = \frac{C_{11} - C_{33}}{2C_{33}},\tag{9}$$

$$\gamma = \frac{C_{66} - C_{44}}{2C_{44}},\tag{10}$$

$$\delta = \frac{(C_{13} + C_{44})^2 - (C_{33} - C_{44})^2}{2C_{33}(C_{33} - C_{44})},\tag{11}$$

where ε is the P-wave anisotropy parameter, γ is the S-wave anisotropy parameter, and δ is the anisotropic parameter can be used to explain the difference between NMO velocity and vertical velocity.

4. Experimental results and analysis

4.1. Range analysis

The range analysis can reveal the effect of influence factors on the properties of artificial shales. The steps of range analysis mainly include: (1) calculate average value k_{ZN} of the indices of each factor under all levels; (2) calculate and compare the range value R_Z and then rank the influence order (Fan et al., 2017; Xi et al., 2019; Yao et al., 2021). The average and range value can be obtained as following:

$$k_{ZN} = \frac{1}{m} \sum_{i=1}^{n} y_{Zi} \tag{12}$$

$$R_Z = R_{\text{max}Z} - R_{\text{min}Z} \tag{13}$$

where i is the experiment number; N is the level number (1, 2, 3, 4), m is the number of experiments for factor Z in N level, n is the total number of tests, m = 4, n = 16 in this study, y_{Zi} is the experimental or calculated results of Sample i influence factor Z.

 k_{ZN} is the average value for the influence factor Z at level N, can evaluate the influence of the factor Z on the experimental results. R_Z is the range value of factor Z, which can evaluate the influence degree of factor Z on the results in the design of this paper, $R_{\text{max}Z} = \max\{k_{Z1}, k_{Z2}, k_{Z3}, k_{Z4}\}$, $R_{\text{min}Z} = \min\{k_{Z1}, k_{Z2}, k_{Z3}, k_{Z4}\}$.

The measured bulk density, porosity and ultrasonic velocities of artificial shales are shown in Table 3. According to the range analysis, the average values of each influence factor on bulk density, porosity at each level are calculated using Eq. (12). The average bulk density decreases with the clay and OM content; while increase with the compaction stress (Fig. 4). The average porosity decreases with the clay content and compaction stress; while increases with the OM content. These results are consistent with previous investigations on natural shales and artificial shales with single variable (Gong et al., 2018; Beloborodov et al., 2018; Xie et al., 2019). Fig. 5 shows the range values of each factor on the bulk density and porosity according to Eqs. (12 and 13), which can be evaluate the influence degree of each factor on the bulk density and porosity. It

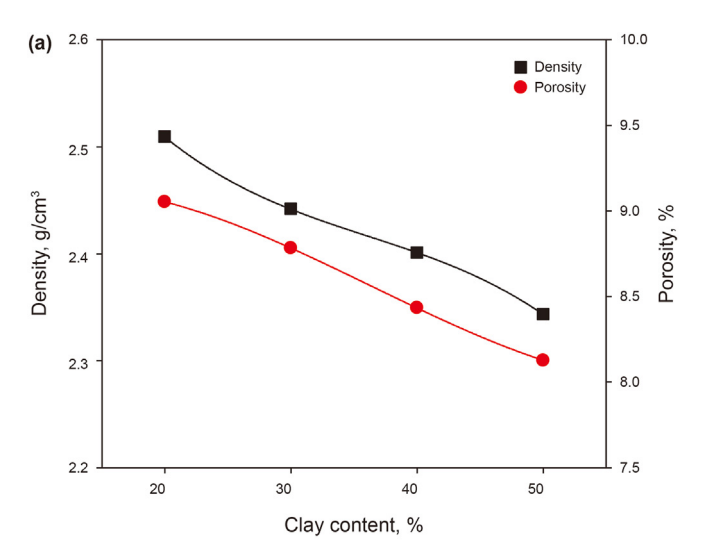
Table 3The measured density, porosity and ultrasonic velocities of artificial shales. The data are original measured values for single sample correspond to samples in Table 2.

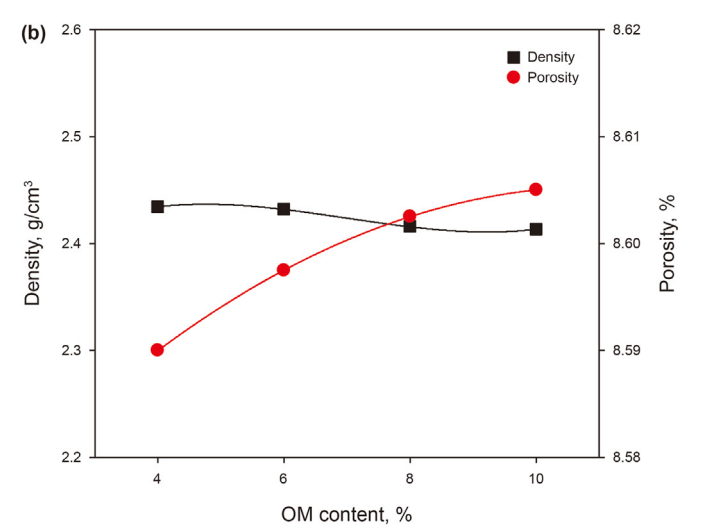
Sample	Density, g/cm ³	Porosity, %	V _{P(0°)}	V _{P(45°)}	V _{P(90°)}	$V_{S(0^\circ)}$	V _{SH(0°)}
A1	2.495	10.15	2842	3154	3465	1845	2150
A2	2.509	9.18	2938	3294	3640	1926	2278
A3	2.513	8.63	2996	3382	3748	1974	2358
A4	2.519	8.25	3038	3453	3840	2017	2440
A5	2.458	8.8	2765	3116	3460	1800	2150
A6	2.418	9.85	2628	2939	3239	1678	1975
A7	2.462	7.99	2885	3320	3721	1921	2357
A8	2.441	8.49	2830	3232	3617	1846	2242
A9	2.415	7.95	2750	3178	3575	1830	2263
A10	2.431	7.65	2808	3258	3675	1880	2346
A11	2.355	9.43	2565	2902	3245	1645	1996
A12	2.403	8.7	2649	3032	3388	1723	2111
A13	2.389	7.46	2752	3203	3620	1825	2296
A14	2.369	7.71	2698	3134	3540	1785	2240
A15	2.332	8.36	2585	2993	3365	1699	2118
A16	2.283	8.98	2495	2864	3215	1640	2030

can be found that the OM content has the smallest effect on both of density and porosity.

As shown in Table 4, the measured ultrasonic velocities of artificial shales follow $V_{P(0^{\circ})} < V_{P(45^{\circ})} < V_{P(90^{\circ})}$ and $V_{SV(0^{\circ})} < V_{SH(90^{\circ})}$, which agrees well with the assumption of TI media. Fig.6 shows the average values for measured ultrasonic velocities with selected influence factors for artificial shales obtained by range analysis, which still follow the sequence $V_{P(0^{\circ})} < V_{P(45^{\circ})} < V_{P(90^{\circ})}$ and $V_{SV(0^{\circ})} < V_{SH(90^{\circ})}$. Fig. 6a shows all average velocities decrease with the clay content, especially at low clay content. Because the elastic moduli of clay minerals are much softer than those of brittle minerals such as quartz, with the increase of clay content, clay particles should become the load-bearing material of skeleton at high clay content, causing the gentler decrease for ultrasonic velocities of samples. Fig. 6b shows ultrasonic velocities slightly decrease with OM content, which mainly attributed to the low elastic moduli of OM. Fig. 6c shows that all average velocities are positively correlated with the compaction stress, especially at low stress. The relatively rapid increase of velocities at low stress can be mainly attributed to the reduce of pore volume caused by the initiation of reorientation and rearrangement of the solid particles. When soft mineral particles such as clay platelets are forced into the interstices between stiff grains such as quartz and even become the load-bearing material of skeleton as the compaction further increase, causing the increase tends of velocities gradually becomes gentler. Note that the variations of velocities caused by the influence factors differ in three orientations, which suggests that the anisotropic velocities should be affected by the influence factors in different ways. Fig. 7 shows the range values for each factor on velocities in three orientations, the OM content has the minimal impact on the velocities compared to clay content and compaction stress; the two latter factors are relative complex to the velocities. Hence, the velocity anisotropy may change depending on the relative velocity variations caused by the influence factors.

To further investigate the impact of the influence factors on the velocity anisotropy parameters, which are calculated from the bulk density and velocities based on Eq. (4)-(11), and the results for single test correspond to samples in Table 2 are shown in Table 4. The minimum velocity anisotropy parameters are observed in Sample A1, while the maximum values are observed in sample A13. Based on data in Table 4, the average velocity anisotropy parameters for the selected influence factors can be obtained based on the range analysis according to Eq. (12)-(13). For the influence factor clay content, OM content and compaction stress, when the level changes from 1 to 4, all average velocity anisotropy parameters





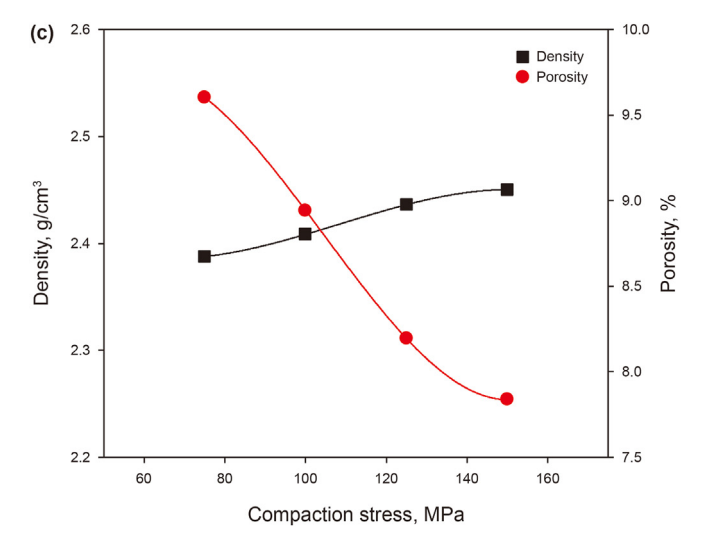


Fig. 4. The influence of factors (a) clay content (b) OM content (c) compaction stress on the average bulk density and porosity obtained by range analysis.

nonlinearly increase, especially with clay content and compaction stress (Fig. 8), which are consistent with the investigations on natural shales and artificial shales with single variable (Vernik and

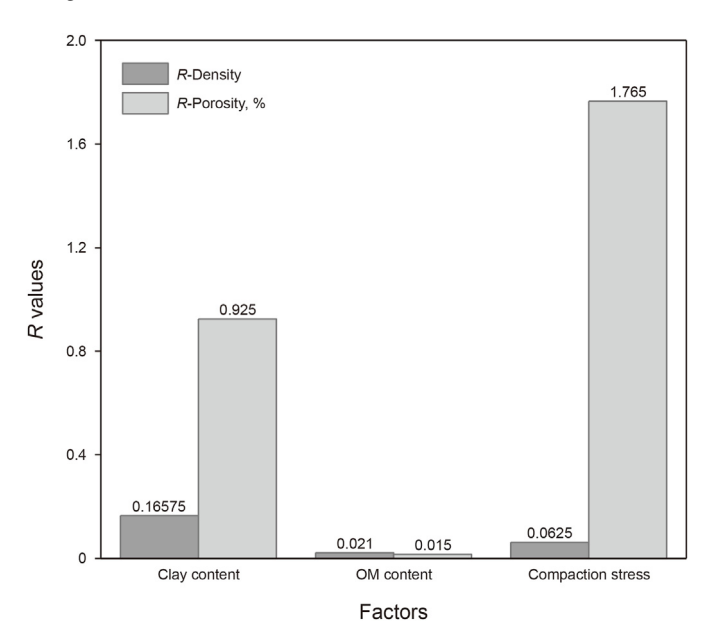


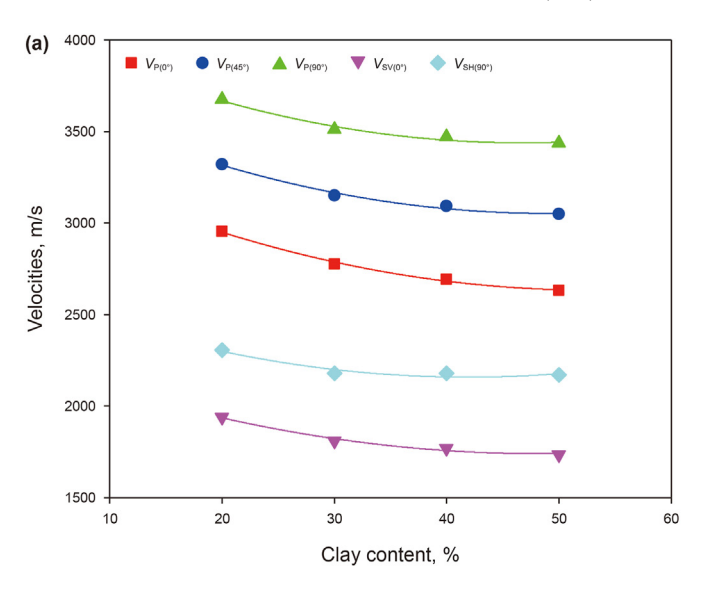
Fig. 5. The range values for each factor on the bulk density and porosity obtained by range analysis.

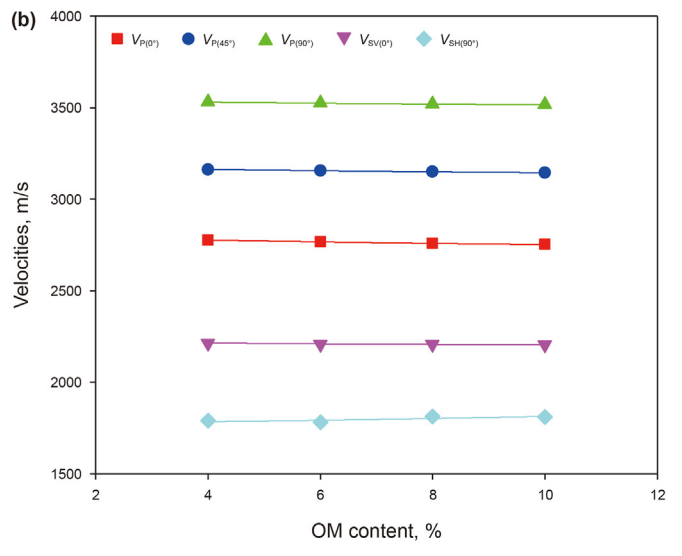
Table 4The calculated velocity anisotropy parameters of artificial shales. The data are original measured values for single sample correspond to samples in Table 2.

Sample	ε	γ	δ
A1	0.243	0.179	0.211
A2	0.267	0.199	0.237
A3	0.283	0.213	0.258
A4	0.299	0.232	0.278
A5	0.283	0.213	0.245
A6	0.260	0.193	0.234
A7	0.332	0.253	0.308
A8	0.317	0.238	0.279
A9	0.345	0.265	0.315
A10	0.356	0.279	0.323
A11	0.300	0.236	0.241
A12	0.318	0.251	0.294
A13	0.365	0.291	0.331
A14	0.361	0.287	0.324
A15	0.347	0.277	0.326
A16	0.330	0.266	0.291

Liu, 1997; Zhao et al., 2016; Ding et al., 2021; Gong et al., 2018; Xie et al., 2019). Note that the average velocity anisotropy parameters slightly increase with the OM content, which is contrary to results from Liu et al. (2022), because the OM in Longmaxi shales is overmature which are differ from our artificial shales. The shape and distribution of OM can be affected by its maturity, the overmature OM in shales displays a patchy distribution, while the low-maturity OM displays preferred lamination (Liu et al., 2022), causing the difference in velocity anisotropy and OM content relationship of shales with different maturity.

Fig. 9 shows the range values for each factor on the P- and S-wave velocity anisotropy parameters, and the range values for each factor follow the sequence: clay content > compaction stress > OM content. For example, the range value for factor clay content is 0.078, and the range value for factor OM content and compaction stress is 0.007 and 0.055, respectively. For the selected influence factors considered in this study, clay content is the dominant influence factor for elastic anisotropy of artificial shales. However, in terms of single sample, the effect of influence factors does not





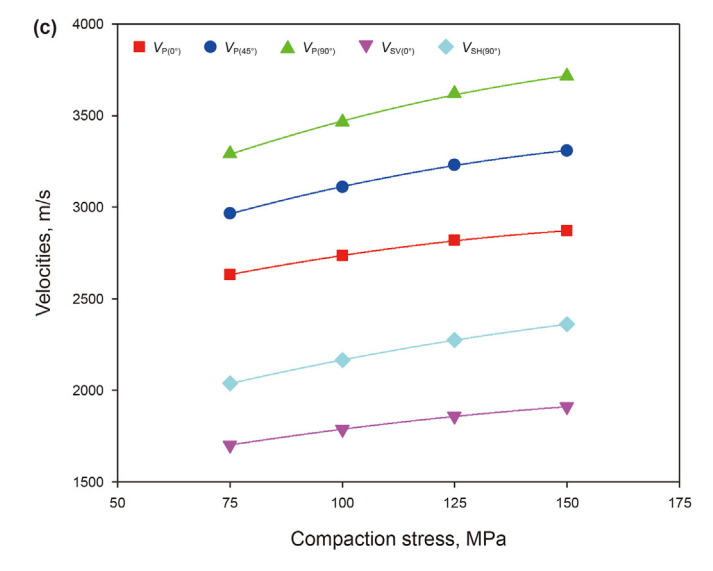


Fig. 6. The influence of factors (a) clay content (b) OM content (c) compaction stress on average the velocities obtained by range analysis.

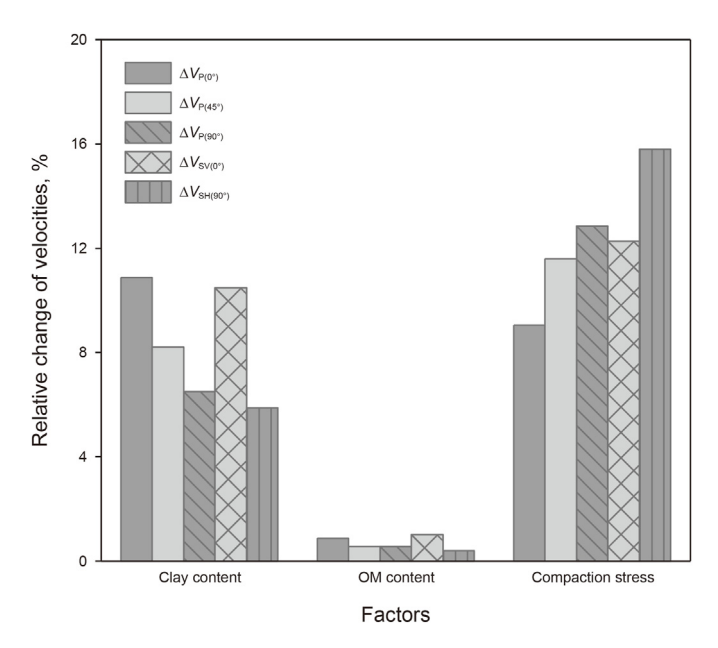


Fig. 7. The range values for each factor on velocities in three orientations obtained by range analysis.

always follow the order obtained from the range analysis for these sixteen artificial shales. For example, with the same OM content, sample A7 contains lower clay content which display higher velocity anisotropy compared to sample A11 because the uniaxial effective stress applied for sample A7 is twice as larger as sample A11, causing a higher degree of lamination for sample A7. From the range analysis, clay content is the dominated factor affecting the elastic anisotropy, and the orientation distribution of clay minerals also has an important influence on shale elastic anisotropy. Therefore, the orientation distribution of clay should be further investigated.

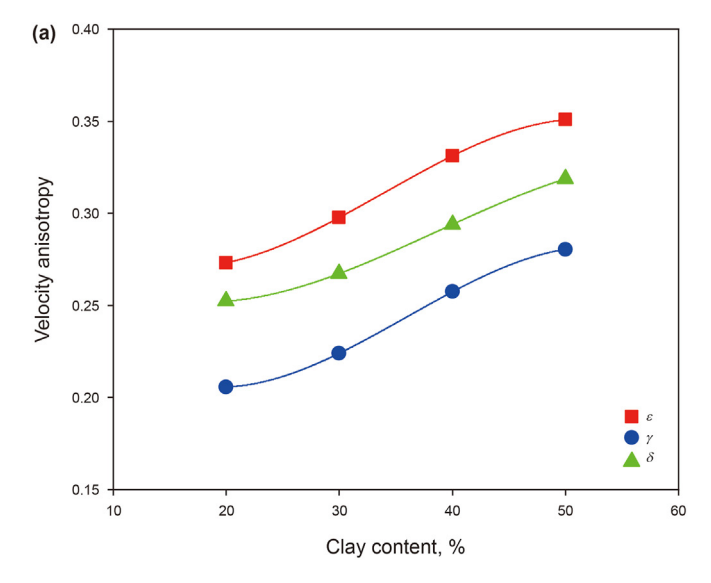
4.2. The compaction effects on the elastic anisotropy

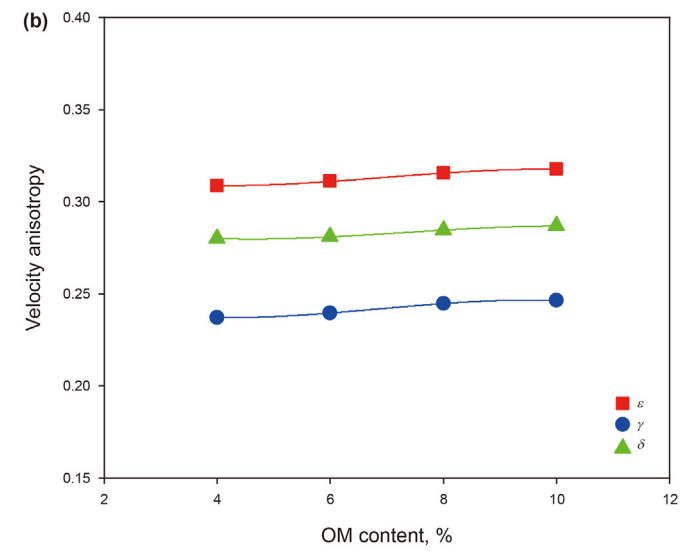
According to Ruud et al. (2003), the compaction factor c is defined as the ratio of the initial to the final layer thickness, which can be calculated as following:

$$c = \frac{h_0}{h} \tag{14}$$

where h_0 and h is the height of artificial shales before and after compaction.

The compaction factors of sixteen artificial shales are obtained from Eq. (14), which have positive correlations with compaction stress and clay content, and the latter is the determinant factor as shown in Fig.10a. With the same clay content, the compaction factor increases with the compaction stress, especially at low clay content. With the compaction stress ranging from 75 to 150 MPa, the compaction factor increases 0.067 for artificial shales containing 20% clay minerals, while it increases 0.024 for artificial shales containing 50% clay minerals. With the same compaction stress, the compaction factor increases with the clay content, especially at low compaction stress. With the clay content ranging from 20% to 50%, the compaction factor increases 0.382 for sample undergoing 75 MPa, while it increases 0.338 for sample undergoing 150 MPa. These observations can be mainly attributed to the mechanical compaction and the change of constitute of rock skeleton caused by variation the in mineral content: the rock skeleton is mainly





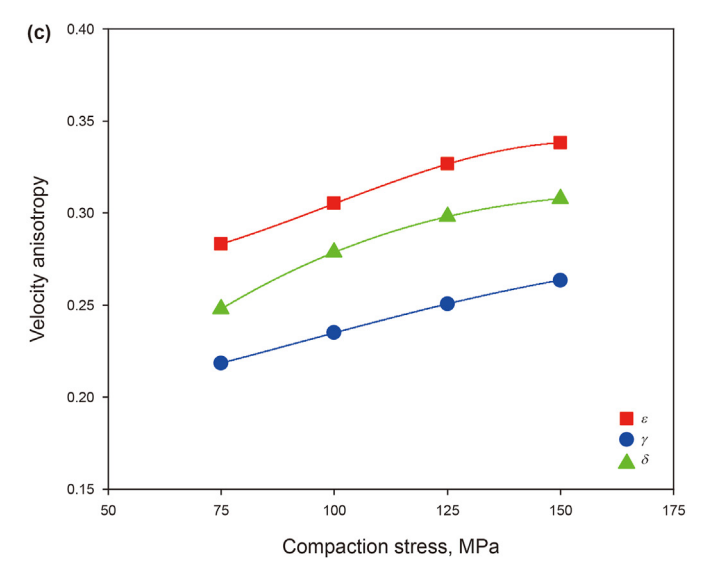


Fig. 8. The influence of factors (a) clay content (b) OM content (c) compaction stress on the average velocity anisotropy parameters obtained by range analysis.

F. Gong, L.-L. Gao, G.-G. Zou et al.

Petroleum Science 20 (2023) 2773–2783

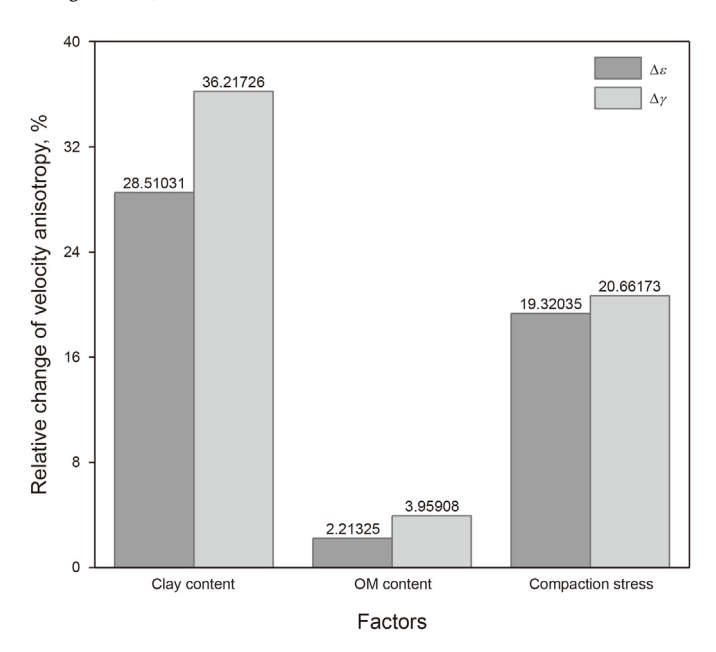


Fig. 9. The range value for each factor on P- and S-wave velocity anisotropy parameters obtained by range analysis.

composed of stiff particles such as quartz particles when the sample contains low clay content; with the increase of clay content, clay particles should become the load-bearing material of skeleton at high clay content which will produce the obstructive effect of compaction, causing the larger increase of compaction factor at low clay content compared that at high clay content. The rearrangement of the solid particles can cause the large increase of compaction factor at low stress. When soft mineral particles such as clay platelets is forced into the interstices between stiff grains such as quartz and even become the constitute of rock skeleton, causing relatively small increase of compaction factor at high stress.

Fig. 10b reveals that the velocity anisotropy parameters are positively correlated with the compaction factors, and the P-wave anisotropy are higher than S-wave anisotropy under the same compaction factor due to most cracks aligned along the bedding plane, which agree well with the observation from Guo et al. (2016). It's well known that shales are much more easily affected by the compaction compared to other sedimentary rocks (Xu and White, 1995). The compaction can reduce the porosity, and also can alter the orientation distribution of the clay platelets, pores and organic matter (Wang, 2002), causing a varied degree of clay orientations in

shales, and eventually leading to the changes in elastic anisotropy of shales. Hence, it is essential to characterize the orientation distribution function (ODF) of the clay platelets in the investigation of shale anisotropy.

4.3. The orientation distribution of clay minerals

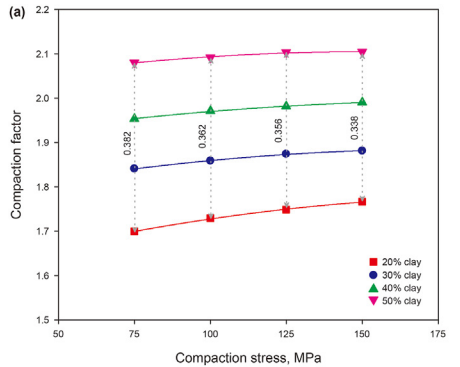
From above analysis, clay content is the dominant factor affecting the elastic anisotropy of artificial shales, but the orientation distribution of clay minerals also has an important influence on the elastic anisotropy. Many studies have investigated the impact of orientation distribution function of the clay platelets on the elastic anisotropy in shales (Sayers and Kachanov, 1995, 2005; Bandyopadhyay, 2009; Pervukhina and Rasolofosaon, 2017; Gong et al., 2020). The compaction ODFs for the alignment of clay platelets can be briefly expressed as following (Owens, 1973; Bandyopadhyay, 2009; Gong et al., 2020):

$$W_C(\theta) = \frac{1}{8\pi^2} \frac{c^2}{(\cos^2 \theta + c^2(1 - \cos^2 \theta))^{\frac{3}{2}}}$$
(15)

where θ represents the angle between the symmetry axis and the normal to the clay platelets, W_C represents the probability density; and c is the compaction factor.

The compaction ODFs can be calculated by combining Eq. (14)-(15), and the compaction ODFs of artificial shales constructed with 20% clay content and with compaction stress 75 MPa before and after compaction (Fig. 11). Before compaction, the compaction factor c is equal to 1, W_C is a constant ($W_I = 1/(8\pi^2)$), indicating the random orientation of the clay platelets, and eventually leading to the overall isotropy of samples. After compaction, the clay platelets will tend to aligned along the bedding plane owing to the applied compaction stress, and this trend will become more prominent when clay content and compaction stress further increase, especially with clay content. These behaviors can verify the correlations between the velocity anisotropy and clay content, compaction stress discussed above.

Assuming the clay platelets and their orientation distribution are transversely isotropic, the effect of their orientation distribution on the elastic stiffnesses of the VTI rock can be completely determined by two ODF coefficients W_{200} and W_{400} (Sayers, 2005; Bandyopadhyay, 2009, Pervukhina and Rasolofosaon, 2017; Gong et al., 2020). Here, the ODF coefficients are calculated using Voigt approximation to the generalized Legendre functions, and coefficients W_{200} and W_{400} of clay plateles in shales are directly converted via elastic anisotropy parameters ε and γ of samples as following (16)—(17).



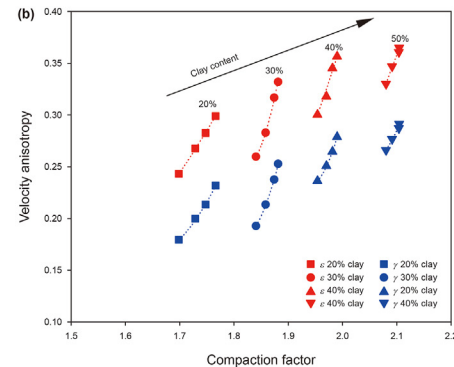


Fig. 10. (a) The compaction factor of artificial shales versus compaction stress, and (b) velocity anisotropy parameters versus compaction factor, red and blue points are P- and S-wave anisotropy, respectively.

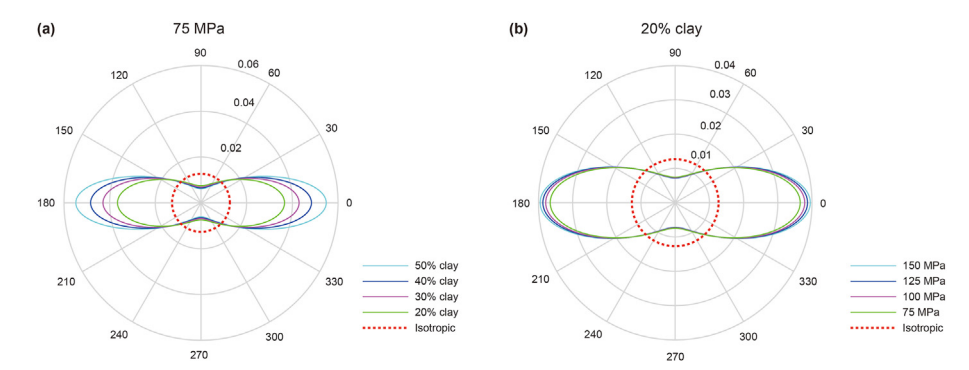


Fig. 11. The compaction ODFs of artificial shales constructed (a) with 20% clay content and (b) with compaction stress 75 MPa before and after compaction. The red dotted line represents the random alignment of clay platelets, and the compaction factor is equal to 1 in this situation.

$$\varepsilon = \frac{(A_{11} - A_{21})W_{200} + (A_{12} - A_{22})W_{400}}{2(A_{10} + A_{21}W_{200} + A_{22}W_{400})},$$
(16)

$$\gamma = \frac{(B_{21} - B_{11})W_{200} + (B_{22} - B_{12})W_{400}}{2(B_{10} + B_{11}W_{200} + B_{12}W_{400})} \tag{17}$$

where the coefficients A and B can be obtained from the elastic constants C_{ij}^0 of the clay platelets, and the details are described in Pervukhina and Rasolofosaon (2017).

The minimum theoretical values of W_{200} and W_{400} : $W_{200} = W_{400} = 0$ suggests a random alignment of clay platelets, leading to the overall isotropy of the rock, corresponding to the compaction factor c is equal to 1 (at the critical porosity) before compaction. While maximum theoretical values of W_{200} and W_{400} : $W_{200}^{\rm max} = \sqrt{10}/8\pi^2 \approx 0.04005$ and $W_{400}^{\rm max} = 3\sqrt{2}/8\pi^2 \approx 0.05373$ represents the perfect alignment of the clay platelets. The elastic constants of clay platelets are taken from the Sayers (2005) with $C_{11}^0=40.0$, $C_{33}^0=16.8$, $C_{55}^0=2.7$, $C_{12}^0=13.8$ and $C_{13}^0=9.0$ GPa to quantitatively evaluate the ODF coefficients, because the stiffness constants of the clay platelets has minor impact on the evaluating results (Gong et al., 2020). Hence, the velocity anisotropy parameters can be converted to the ODF coefficients W_{200} and W_{400} using Eqs. 16 and 17, the detail can be found in Pervukhina and Rasolofosaon (2017). Fig. 12 shows the relations between the ODF coefficients and the velocity anisotropy parameters, the P-wave and S-wave anisotropy parameters display a good linear relation, and both of them increase with the two compaction ODF. The values of ODF coefficients are positive and are much smaller than the maximum theoretical value. Fig. 12 also can directly illustrate the

relation between the velocity anisotropy and clay content discussed above, the samples containing high clay content can cause low velocity anisotropy due to the low degree of alignment of clay platelets caused by the compaction, which are consistent with the observation from Liu et al. (2022).

Fig. 13 shows the relation between ODF coefficients and compaction stress for sixteen artificial shales. The ODF coefficients are combinedly affected by the clay content and compaction stress, and W_{200} are much more sensitive to the clay content and compaction stress compared to the W_{400} . Further, both W_{200} and W_{400} have positive corrections with the compaction stress, and the increase tends to be greater at lower clay content compared that at higher clay content. With the same compaction stress, the shales containing high clay content possess large W_{200} and W_{400} , which correspond to the high elastic anisotropy parameters as shown in Table 4.

Compared with natural shales, the artificial shales have the advantages of repeatability of process, controllability of the variables. However, the compaction process of artificial shale is pure mechanical excluding chemical compaction process, causing the velocities of artificial shales are relatively lower than velocities of natural shale. Nevertheless, the results in this paper still can contribute to understanding how multiple influence factors affect the elastic anisotropy of shales and may be used to estimate how the elastic anisotropy evolve due to burial of the low-maturity or maturity shale reservoir. Further, the results in this paper can provide a critical rock physics basis and data support for quantitative interpretation and reservoir prediction of the low-maturity or maturity shales such as Yanchang shales. For example, the detailed characterization of clay platelet ODFs, and the relations between the elastic anisotropy and the influence factors can

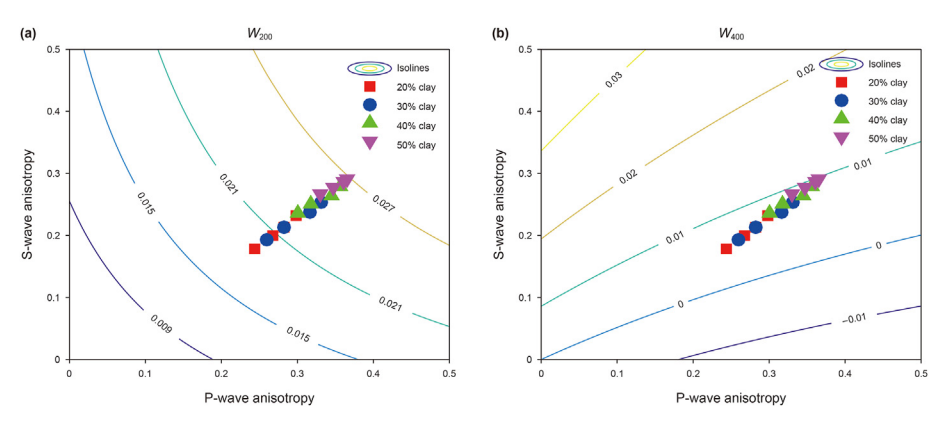


Fig. 12. Both P- and S-wave anisotropy of sixteen artificial shales superimposed with (a) W_{200} and (b) W_{400} isolines.

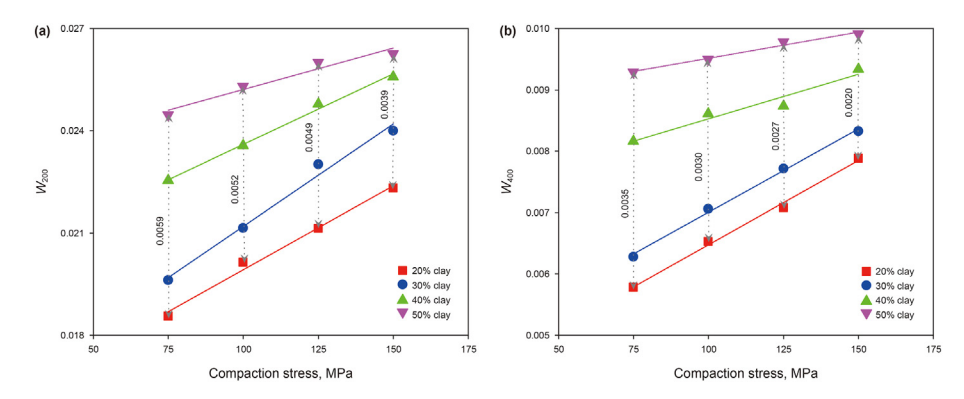


Fig. 13. The ODF coefficients (a) W_{200} and (b) W_{400} of sixteen artificial shales versus the compaction stress.

establish a baseline for predicting elastic properties of shales, which are essential for reservoir prediction. Note that the influence of organic matter maturity on the intrinsic elastic anisotropy and the effect of cracks on the stress-induced elastic anisotropy of shales are not investigated in this study due to the material limitation, which will be comprehensively investigated in another paper.

5. Conclusions

To analyze the effect of multiple influence factors for intrinsic elastic anisotropy of shales, sixteen artificial shales are constructed based on the orthogonal test method, three factors including clay content, OM content and compaction stress are selected as independent variables. According the range analysis, the average velocity anisotropy parameters have positive correlations with the clay content, OM content and compaction stress, and the orders of the selected influence factors follow the sequence clay content > compaction stress > OM content for velocity anisotropy. Note that the effects of influence factors on the individual sample dose not always follow the order obtained from the range analysis, because orientation distribution of clay minerals also has an important influence on shale elastic anisotropy. The compaction factors have positive correlations with compaction stress and clay content, especially at low clay content and compaction stress, which can be mainly attributed to the mechanical compaction and the change of constitute of rock skeleton caused by variation the in mineral content. The clay platelets orientation distribution of the artificial shales is evaluated by a theoretical model, the ODF coefficients are obviously affected by the clay content and compaction stress, and W_{200} are much more sensitive to these factors compared to the W_{400} .

Declaration of competing interest

The authors declare that they have no known competing financial interests or personal relationships that could have appeared to influence the work reported in this paper.

Acknowledgement

This study is supported by the National Natural Science Fund Projects (42104107), the Fundamental Research Funds for the Central Universities (2022XJDC06). The data associated with this research are available and can be obtained by contacting the corresponding author.

References

Allan, A.M., Kanitpanyacharoen, W., Vanorio, T., 2015. A multiscale methodology for the analysis of velocity anisotropy in organic-rich shale. Geophysics 80 (4), C73—C88. https://doi.org/10.1190/geo2014-0192.1.

Altowairqi, Y., Rezaee, R., Evans, B., et al., 2015. Shale elastic property relationships as a function of total organic carbon content using synthetic samples. J. Petrol. Sci. Eng. 133, 392–400. https://doi.org/10.1016/j.petrol.2015.06.028.

Bandyopadhyay, K., 2009. Seismic Anisotropy-Geological Causes and its Implications to Reservoir Geophysics. Ph.D. thesis. Stanford University.

Beloborodov, R., Pervukhina, M., Lebedev, M., 2018. Compaction trends of full stiffness tensor and fluid permeability in artificial shales. Geophys. J. Int. 212 (3), 1687–1693. https://doi.org/10.1093/gii/ggx510.

1687–1693. https://doi.org/10.1093/gji/ggx510. Beloborodov, R., Pervukhina, M., Luzin, V., et al., 2016. Compaction of quartz-kaolinite mixtures: the influence of the pore fluid composition on the development of their microstructure and elastic anisotropy. Mar. Petrol. Geol. 78, 426–438. https://doi.org/10.1016/j.marpetgeo.2016.09.030.

Dewhurst, D.N., Siggins, A.F., 2006. Impact of fabric, microcracks and stress field on shale anisotropy. Geophys. J. Int. 165 (1), 135–148. https://doi.org/10.1111/j.1365-246X.2006.02834.x.

Ding, P.B., Gong, F., Zhang, F., Li, X.Y., 2021. A physical model study of shale seismic responses and anisotropic inversion. Petrol. Sci. 18 (4), 1059–1068. https:// doi.org/10.1016/j.petsci.2021.01.001.

Fan, P.X., Yan, Z.C., Wang, M.Y., et al., 2017. Recyclable resin-based analogue material for brittle rocks and its application in geomechanical model test. Arabian J. Geosci. 10, 29. https://doi.org/10.1007/s12517-016-2814-y.

Gong, F., Di, B.R., Wei, J.X., 2018. Ultrasonic velocity and mechanical anisotropy of synthetic shale with different types of clay minerals. Geophysics 83 (2), MR57–MR66. https://doi.org/10.1190/geo2016-0590.1.

Gong, F., Di, B.R., Zeng, L.B., et al., 2020. Static and dynamic linear compressibility of dry artificial and natural shales under confining pressure. J. Petrol. Sci. Eng. 192, 107242. https://doi.org/10.1016/j.petrol.2020.107242.

Guo, Z.Q., Liu, C., Liu, X.W., 2016. Research on anisotropy of shale oil reservoir based on rock physics model. Appl. Geophys. 13 (2), 382—392. https://doi.org/10.1007/s11770-016-0554-0.

Hornby, B.E., 1998. Experimental laboratory determination of the dynamic elastic properties of wet, drained shales. J. Geophys. Res. 103 (B12), 29945–29964. https://doi.org/10.1029/97JB02380.

Kawamura, K., Ogawa, Y., 2004. Progressive change of pelagic clay microstructure during burial process: examples from piston cores and ODP cores. Mar. Geol. 207 (1–4), 131–144. https://doi.org/10.1016/j.margeo.2004.03.016.

Li, Y., Guo, Z.Q., Liu, C., al, rt, 2015. A rock physics model for the characterization of organic-rich shale from elastic properties. Petrol. Sci. 12, 264–272. https://doi.org/10.1007/s12182-015-0029-6.

Liu, Z.C., Peng, R., Li, X.Y., et al., 2022. Wave velocity in shale in the wufeng-Longmaxi formation in Sichuan basin. J. Geophys. Eng. 19 (3), 283–294. https://doi.org/10.1093/jge/gxac011.

Luan, X.Y., Di, B.R., Wei, J.X., et al., 2016. Creation of synthetic samples for physical modelling of natural shale. Geophys. Prospect. 64 (4), 898–914. https://doi.org/ 10.1111/1365-2478.12382.

Mavko, G., Mukerji, T., Dvorkin, J., 2020. The Rock Physics Handbook. Cambridge university press, Cambridge, pp. 1–716. https://doi.org/10.1017/9781108333016. Mondol, N.H., Bjørlykke, K., Jahren, J., 2008. Experimental compaction of clays: relationship between permeability and petrophysical properties in mudstones. Petrol. Geosci. 14 (4), 319–337. https://doi.org/10.1144/1354-079308-773.

Mondol, N.H., Bjørlykke, K., Jahren, J., et al., 2007. Experimental mechanical compaction of clay mineral aggregates—changes in physical properties of mudstones during burial. Mar. Petrol. Geol. 24 (5), 289–311. https://doi.org/ 10.1016/j.marpetgeo.2007.03.006.

Moyano, B., Spikes, K.T., Johansen, T.A., et al., 2012. Modeling compaction effects on the elastic properties of clay-water composites. Geophysics 77 (5), D171–D183. https://doi.org/10.1190/geo2011-0426.1.

Owens, W.H., 1973. Strain modification of angular density distributions.

- Tectonophysics 16 (3–4), 249–261. https://doi.org/10.1016/0040-1951(73)
- Pan, X.P., Zhang, G.Z., Yin, X.Y., 2018. Azimuthally pre-stack seismic inversion for orthorhombic anisotropy driven by rock physics. Sci. China Earth Sci. 61, 425–440. https://doi.org/10.1007/s11430-017-9124-6.
- Pervukhina, M., Rasolofosaon, P.N.J., 2017. Compaction trend versus seismic anisotropy in shaly formations. Geophys. Prospect. 65, 1351–1365. https://doi.org/10.1111/1365-2478.12486.
- Prasad, M., Mba, K.C., McEvoy, T.E., et al., 2011. Maturity and impedance analysis of organic-richshales. SPE Reservoir Eval. Eng. 14 (5), 533–543. https://doi.org/10.2118/123531-PA.
- Ruud, B.O., Jakobsen, M., Johansen, T.A., 2003. Seismic Properties of Shales during Compaction. SEG Technical Program Expanded Abstracts. pp. 1294—1297.
- Sarout, J., Guéguen, Y., 2008. Anisotropy of elastic wave velocities in deformed shales: Part 1 — experimental results. Geophysics 73 (5), D75—D89. https:// doi.org/10.1190/1.2952744.
- Sayers, C.M., 2005. Seismic anisotropy of shales. Geophys. Prospect. 53 (5), 667–676. https://doi.org/10.1111/j.1365-2478.2005.00495.x.
- Sayers, C.M., 2013. The effect of anisotropy of the Young's moduli and Poisson's ratios shales. Geophys. Prospect. 61 (2), 416–426. https://doi.org/10.1111/j.1365-2478.2012.01130.x.
- Sayers, C.M., Guo, S.G., Silva, J., 2015. Sensitivity of the elastic anisotropy and seismic reflection amplitude of the Eagle Ford Shale to the presence of kerogen. Geophys. Prospect. 63 (1), 151–165. https://doi.org/10.1111/1365-2478.12153.
- Sayers, C.M., den Boer, L.D., 2019. The impact of different clay minerals on the anisotropy of clay matrix in shale. Geophys. Prospect. 67 (9), 2298–2318. https://doi.org/10.1111/1365-2478.12829.
- Sayers, C.M., Kachanov, M., 1995. Microcrack-induced elastic wave anisotropy of brittle rocks. J. Geophys. Res. Solid Earth 100 (B3), 4149—4156. https://doi.org/ 10.1029/94JB03134.
- Sondergeld, C.H., Rai, C.S., 2011. Elastic anisotropy of shales. Lead. Edge 30 (3), 324–331. https://doi.org/10.1190/1.3567264.
- Sone, H., Zoback, M.D., 2013. Mechanical properties of shale—gas reservoir rock-s—Part 1: static and dynamic elastic properties and anisotropy. Geophys. Nor. 78 (5), 381–392. https://doi.org/10.1190/geo2013-0050.1.
- Thomsen, L., 1986. Weak elastic anisotropy. Geophysics 51 (10), 1954–1966. https://doi.org/10.1190/1.1442051.

- Vasin, R.N., Wenk, H.R., Kanitpanyacharoen, W., et al., 2013. Elastic anisotropy modeling of Kimmeridge shale. J. Geophys. Res. Solid Earth 118 (8), 3931–3956. https://doi.org/10.1002/jgrb.50259.
- Vernik, L., Liu, X.Z., 1997. Velocity anisotropy in shales. A petrophysical study: Geophysics 62 (2), 521–532. https://doi.org/10.1190/1.1444162.
- Vernik, L, Nur, A., 1992. Ultrasonic velocity and anisotropy of hydrocarbon source rocks. Geophysics 57 (5), 727–735. https://doi.org/10.1190/1.1443286.
- Voltolini, M., Wenk, H.-R., Mondol, N.H., et al., 2009. Anisotropy of experimentally compressed kaolinite-illite-quartz mixtures. Geophysics 74 (1), D13–D23. https://doi.org/10.1190/1.3002557.
- Wang, Z., 2002. Seismic anisotropy in sedimentary rocks, part 2: laboratory data. Geophysics 67 (5), 1423–1440. https://doi.org/10.1190/1.1512743.
- Wenk, H.R., Lonardelli, I., Franz, H., et al., 2007. Preferred orientation and elastic anisotropy of illite-rich shale. Geophysics 72 (2), E69–E75. https://doi.org/ 10.1190/1.2432263.
- Xi, H., Zhang, H.H., He, Y.L., et al., 2019. Sensitivity analysis of operation parameters on the system performance of organic rankine cycle system using orthogonal experiment. Energy 172, 435–442. https://doi.org/10.1016/j.energy.2019.01.072.
- Xie, J.Y., Cao, J.X., Schmitt, D.R., et al., 2019. Effects of kerogen content on elastic properties-based on artificial organic-rich shale (AORS). J. Geophys. Res. Solid Earth 124 (12), 12660–12678. https://doi.org/10.1029/2019JB017595.
- Xu, S., White, R.E., 1995. A new velocity model for clay-sand mixtures. Geophys. Prospect. 43 (1), 91–118. https://doi.org/10.1111/j.1365-2478.1995.tb00126.x.
- Yang, X.G., Guo, S.B., 2020. Porosity model and pore evolution of transitional shales: an example from the Southern North China Basin. Petrol. Sci. 17, 1512–1526. https://doi.org/10.1007/s12182-020-00481-7.
- Yao, Z.P., Liu, J.Q., Qiu, Z.Z., et al., 2021. Numerical investigation of 700°C boiler flue gas thermal deviation based on orthogonal experiment. Fuel 295 (1), 120510. https://doi.org/10.1016/j.fuel.2021.120510.
- Yenugu, M.R., 2014. Elastic, Microstructural and Geochemical Characterization of Kerogen Maturity for Shales. Ph.D. thesis. Houston University.
- Zargari, S., Prasad, M., Mba, K.C., et al., 2013. Organic maturity, elastic properties, and textural characteristics of self resourcing reservoirs. Geophysics 78, D223–D235. https://doi.org/10.1190/geo2012-0431.1.
- Zhao, L.X., Qin, X., Han, D.H., et al., 2016. Rock-physics modeling for the elastic properties of organic shale at different maturity stages. Geophysics 81 (5), D527–D541. https://doi.org/10.1190/geo2015-0713.1.